Inorganic Chemistry

ARTICLE

pubs.acs.org/IC

Synthesis, Structure, and Magnetic Properties of the $NaCoXO_4F \cdot 2H_2O$ Phases Where X = S and Se

B. C. Melot,[†] J-N. Chotard,[†] G. Rousse,[‡] M. Ati,[†] M. Reynaud,[†] and J-M. Tarascon*[,†]

[†]Laboratoire de Réactivité et Chimie des Solides, CNRS UMR 6007, Université de Picardie Jules Verne, 33 Rue Saint-Leu, 80039 Amiens, France

[‡]Institut de Minéralogie et de Physique des Milieux Condensés (IMPMC) UMR 7590 CNRS, Université Pierre et Marie Curie (UPMC), Case courrier 115, 4 Place Jussieu, 75252 Paris Cedex 05, France

Supporting Information

ABSTRACT: A novel hydrated fluoroselenate $NaCoSeO_4F \cdot 2H_2O$ has been synthesized, and its structure determined. Like its sulfate homologue, $NaCoSO_4F \cdot 2H_2O$, the structure contains one-dimensional chains of corner-sharing MO_4F_2 octahedra linked together through F atoms sitting in a trans configuration with respect to each other. The magnetic properties of the two phases have been investigated using powder neutron diffraction and susceptibility measurements which indicate antiferromagnetic ordering along the length of the chains and result in a G-type antiferromagnetic ground state. Both compounds exhibit a Néel temperature near 4 K, and undergo a field-induced magnetic phase transition in fields greater than 3 kOe.

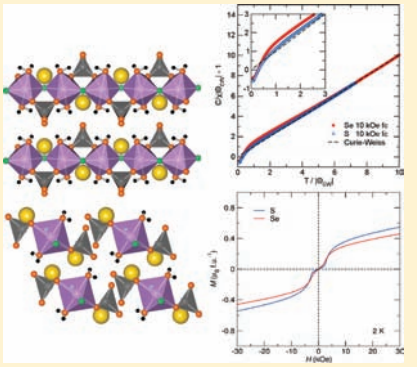

INTRODUCTION

In recent years research on Li-ion batteries has rekindled interest in the chemistry of fluorine as most electrolytes presently in use rely upon Li-based fluoride salts. From the point of view of the positive electrode, F-based compounds are beginning to draw increased attention because of their ability to display greater operating potentials than oxide-based electrodes. Early work by Férey et al. demonstrated the rich structural diversity of fluorophosphates.[1,2] Newer fluorophosphate-based phases, such as Na_2FePO_4F and $LiMPO_4F$ (M = Co, Fe, Ni, Mn), or oxyfluorides like FeOF and BiOF-based electrodes, which operate through insertion and conversion reactions, have been reported in the literature, respectively.[3,4] More recently, we have characterized a new family of fluorosulfates $(Li,Na)MSO_4F$ (M = Fe, Co, Ni, Mg) having the tavorite structure, where the $LiFeSO_4F$ phase shows attractive electrochemical performances in Li-based batteries with sustained reversible capacities of 140 mA h g^{-1} at an average potential of 3.6 V.[5]

These new fluorosulfate phases, made either via ionothermal, ceramic, or polymer process, were found to decompose at temperatures greater than 350 °C in addition to being unstable in the presence of water. This poor thermodynamic stability comes as somewhat of a surprise given that the mineral Uklonskovite, $NaMgSO_4F \cdot 2H_2O$,[6] has been reported in the literature. Aware of the existence of this compound, we attempted to synthesize more novel hydrated fluorosulfates and successfully obtained $NaMSO_4F \cdot 2H_2O$ where M is the Ni, Co, and Fe.

Herein we present a study of the new fluoroselenate, $NaCoSeO_4F \cdot 2H_2O$, and report its synthesis, structure, and magnetic properties together with that of its counterpart, $NaCoSO_4F \cdot 2H_2O$. Both compounds display complex magnetic behavior at temperatures below 4 K with a field-induced transition occurring in magnetic fields stronger than 3 kOe. Using powder neutron diffraction experiments we propose a possible model for the ground state magnetic structure.

EXPERIMENTAL SECTION

Synthesis. $NaCoSO_4F \cdot 2H_2O$ was prepared via a previously established protocol.[7] Stoichiometric amounts of commercially available $CoSO_4 \cdot 6H_2O$ and NaF were separately dissolved in enough water to obtain transparent, fully dissolved solutions. The two solutions were then mixed and heated to 80 °C while stirring for approximately 5 h until roughly 90% of the water had evaporated. The product was collected by mixing the resulting solution with a large excess of ethanol, centrifuging, and air drying at 100 °C for 1 h. A similar procedure, using D_2O rather than H_2O medium, was used to prepare the deuterated sample, $NaCoSO_4F \cdot 2D_2O$, which was studied in the neutron diffraction experiments.

For the synthesis of the selenate-based phase, the precursor $CoSeO_4 \cdot 6H_2O$ phase was prepared following a procedure reported in the literature.[8] A solution of selenic acid (2.559 g of SeO_2 dissolved in

Received: April 6, 2011
Published: July 12, 2011

Table 1. Lattice and Figure of Merits of the Rietveld Refinements for the Title Compounds[a]

	$NaCoSO_4F \cdot 2D_2O$	$NaCoSeO_4F \cdot 2H_2O$
space group	$P2_1/m$	$P2_1/m$
a (Å)	5.73991(6)	5.8235(3)
b (Å)	7.32250(7)	7.4099(3)
c (Å)	7.19288(8)	7.3973(4)
β (deg)	113.512(1)	114.183(2)
V (Å^3)	277.221(5)	291.19(2)
χ^2	2.04	3.31
R_{Bragg}%	3.58	6.42

[a] For the sulfate phase, values are taken from the results of the refinement of the neutron diffraction data on the deuterated sample.

50 mL of 30% H_2O_2) was neutralized at 70 °C with $Co_2(CO_3)_x(OH)_y$ which was prepared in-house according to another previously reported procedure.[9] The solution was allowed to slowly crystallize over several days at room temperature so as to produce large-faceted crystals of the red $CoSeO_4 \cdot 6H_2O$ phase. Once obtained, the product was reacted with a stoichiometric amount of NaF to produce $NaCoSeO_4F \cdot 2H_2O$ at 80 °C as described above for the sulfate-based phase. Attempts to recrystallize the selenate phase by complete water evaporation mainly resulted in multiphase powders, so instead recrystallization was done by addition of an excess of ethanol. The resulting powder was dark red as opposed to pink for the sulfate.

Both products were analyzed by powder X-ray diffraction (XRD). A Bruker D8 diffractometer with Cu Kα radiation (λ_1 = 1.54056 Å, λ_2 = 1.54439 Å) equipped with a Lynxeye detector was used for the selenate sample whereas a Bruker D8 diffractometer with Co Kα radiation (λ_1 = 1.78897 Å, λ_2 = 1.79285 Å) equipped with a Vantec detector was used for the sulfate sample. Neutron diffraction data were collected on the D2B powder diffractometer at the Institut Laue-Langevin (ILL), France using wavelengths of 1.594 Å and 2.398 Å. The D2B diffractometer has a very high resolution at 1.594 Å and was therefore used to precisely refine the nuclear structure of the deuterated sample. A wavelength of 2.398 Å was also used to more accurately determine the magnetic structure by enhancing the range of available peaks at high d-spacings. All refinements of the nuclear and/or magnetic structure presented used the FullProf suite of programs[10] using the Rietveld method.[11]

The temperature dependence of the direct current magnetization was measured using a Quantum Design MPMS 5XL SQUID magnetometer. All powders were embedded in paraffin wax and deposited in gel caps so as to prevent the rotation of the particles in large magnetic fields. Scanning electron microscopy images (not shown) were recorded with an FEI Quanta 200F operating at 20 kV under low vacuum to avoid a charging effect and fitted with an EDAX Energy Dispersive Spectrometer (EDS). The measurements to determine the sample elemental makeup were repeated in at least 10 different spots of the samples with the size of the probe set to 1 μm to probe a depth of 1 μm below the surface. The elemental composition was determined by energy dispersive spectroscopy (EDS) analysis with the calculated atomic percents being Na 10(2)%, Co 10(1)%, Se 10(1)%, F 10(3)%, O 60(5)% in agreement with the overall formula $NaCoSeO_4F \cdot 2H_2O$. These reported values are an average of 10 measurements with the estimated error being the largest values. Thermal gravimetric analysis (TGA) found the amount of water present to be nearly 1.95, which is in good agreement with the expected value of 2.

In a previous report,[12] we presented the crystal structure of $NaCoSO_4F \cdot 2H_2O$, but the position of the hydrogen atoms remained ambiguous. We have therefore collected powder neutron diffraction patterns on a deuterated sample and now present the complete crystal structure for the sulfate. From the resulting refinement against the data the deuterium atoms were found to be sitting on the 4f Wyckoff position of space group $P2_1/m$ (Table 1 and Table 2). The structure of the selenate, which bears great similarities with that of the sulfate, was determined by refining the structure against powder XRD data (see Figure 1) starting with the atomic positions and cell parameters obtained for the sulfate phase. The cell parameters obtained from the refinement are shown in Table 1 and the atomic positions are reported in Table 3. A Bond Valence Sum analysis (BVS)[29] was done and is in good agreement with what is expected as shown in Table 2. Both phases crystallize in the $P2_1/m$ space group like the previously reported $NaMgSO_4F \cdot 2H_2O$. The unit cell volume increases by 5% in going from the S to the Se-based phases, which is consistent with the ionic radius of Se, 0.50 Å, being larger than that of S, 0.37 Å.

The Uklonskovite structure consists of MO_4F_2 octahedra linked together at their corners through F atoms which are oriented in a trans

Table 2. Atomic Coordinates of $NaCoSO_4F \cdot 2D_2O$ Resulting from the Rietveld Refinement against the Room Temperature Powder Neutron Diffraction Patterns Obtained on the D2B High Resolution Diffractometer[a]

atom	Wyckoff position	x	y	z	BVS	B (Å^2)
Na	2e	0.1214(12)	$^1/_4$	0.6963(9)	1.00(2)	1.00(10)
Co	2d	$^1/_2$	0	$^1/_2$	2.06(2)	0.47(11)
F	2e	0.3670(6)	$^1/_4$	0.5180(6)	0.95(2)	0.797(15)
S	2e	0.6492(12)	$^1/_4$	0.1947(9)	5.76(5)	0.22(9)
O1	4f	0.7044(5)	0.0839(4)	0.3275(3)	1.82(2)	0.797(15)
O2	2e	0.8267(6)	$^1/_4$	0.0914(5)	2.46(4)	0.797(15)
O3	2e	0.3824(6)	$^1/_4$	0.0468(6)	1.71(3)	0.797(15)
D1	4f	0.2049(6)	0.5877(4)	0.1232(5)	0.88(2)	3.50(5)
D2	4f	0.0769(6)	0.0694(4)	0.1957(4)	0.90(2)	3.50(5)
O4	4f	0.1692(5)	0.5458(3)	0.2403(4)	1.81(2)	0.797(15)

[a] The bond valence sum (BVS) is indicated for each atom.

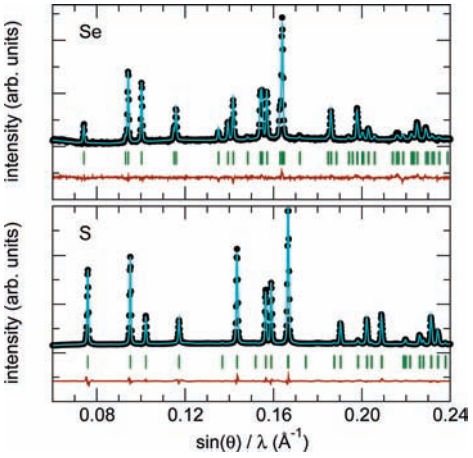

Figure 1. Rietveld refinements of the powder XRD patterns collected at room temperature (upper panel: $NaCoSeO_4F \cdot 2H_2O$, lower panel: $NaCoSO_4F \cdot 2H_2O$). The black dots are experimental points while the blue and red lines are the calculated fit and the difference curve, respectively. Remember that the selenate pattern was collected with a Cu source whereas the sulfate pattern was collected using a Co source. The x-axis is therefore presented in a way that allows for a more direct comparison of the patterns.

dx.doi.org/10.1021/ic200700r |Inorg. Chem. 2011, 50, 7662–7668

Table 3. Atomic Coordinates of $NaCoSeO_4F \cdot 2H_2O$ Resulting from the Rietveld Refinement against the Laboratory XRD Patterns[a]

atom	Wyckoff position	*x*	*y*	*z*
Na	2e	0.122(2)	$^1/_4$	0.687(2)
Co	2*d*	$^1/_2$	0	$^1/_2$
F	2*e*	0.378(3)	$^1/_4$	0.522(2)
Se	2*e*	0.6321(8)	$^1/_4$	0.1824(8)
O1	4*f*	0.735(2)	0.101(2)	0.325(2)
O2	2*e*	0.846(4)	$^1/_4$	0.069(3)
O3	2*e*	0.351(4)	$^1/_4$	0.017(3)
O4	4*f*	0.172(3)	0.538(2)	0.240(2)

[a] Note that thermal parameters could not be accurately obtained because of the small angular region of the available data set. They have therefore been omitted.

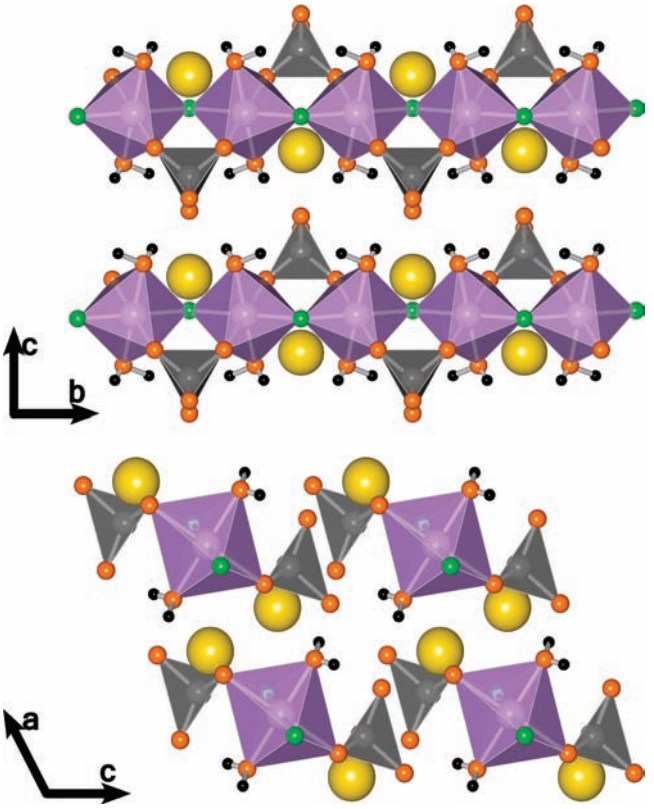

Figure 2. Crystal structure of $NaCoSeO_4F \cdot 2H_2O$ along the *a* axis (top panel) and along the *b* axis (bottom panel). Co atoms in purple, F in green, O in orange, Na in yellow, H in black, and Se in dark gray. The structure is composed of octahedra which share corners through F atoms (in green) which sit trans with respect to each other to form straight chains which run along the *b*-axis. Note that the position of the hydrogen atoms was not directly determined for the selenate phase, but since the compound is isostructural to $NaCoSO_4F \cdot 2H_2O$ we show the relative orientation for that phase.

configuration with respect to each other giving rise to straight chains which run along the *b*-axis. Among the four oxygen atoms constituting the equatorial plane of the octahedra, those denoted as O4 are part of coordinated H_2O molecules while the other two, denoted as O1, are part of the XO_4 tetrahedra (see Figure 2). These XO_4 units contain two double bonds and two single bonds as is necessary to satisfy the octet of

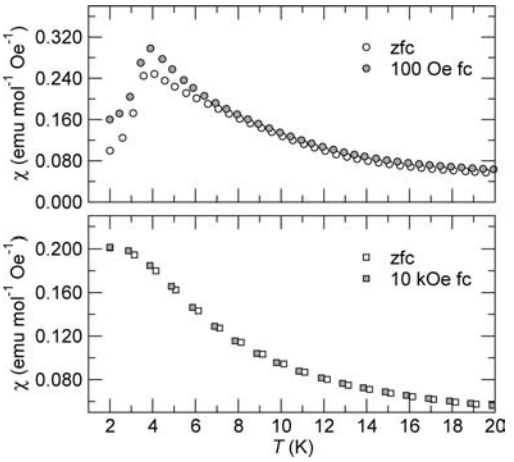

Figure 3. Temperature-dependent magnetic susceptibility of $NaCoSO_4F \cdot 2H_2O$. The top panel was collected in a small field of 100 Oe whereas the bottom panel was collected in a moderately large field of 10 kOe. Note how the sharp peak at 4 K is suppressed in larger fields.

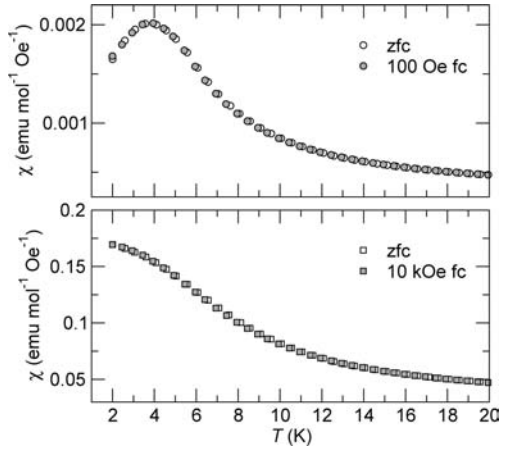

Figure 4. Temperature-dependent magnetic susceptibility of $NaCoSeO_4F \cdot 2H_2O$. The top panel was collected in a small field of 100 Oe whereas the bottom panel was collected in a moderately large field of 10 kOe. Note that the peak at 4 K is significantly smoother than that of the sulfate phase. However, it is suppressed in larger fields in a similar fashion.

the *X* atoms. In the selenate the double-bonds correspond to the Se−O1 distances (1.49 Å compared to 1.76 Å and 1.59 Å for the Se−O2 and Se−O3 respectively) and are oriented such that they bridge the nearest neighboring octahedron along the length of the chains. In contrast, the double-bonds in the sulfate appear randomly oriented since all the S−O bond lengths are very similar (1.50 Å, 1.48 Å, and 1.48 Å for the S−O1, S−O2, and S−O3 distances, respectively). The O2 oxygen of the XO_4 units, which is not directly coordinated to either Co or Na, experiences a hydrogen bonding interaction with the coordinated water molecules in the neighboring chains. The Na atoms sit in tetrahedral sites and are coordinated by three oxygens and one fluorine.

Regarding the electrochemistry and ionic conductivity, the $NaCoSeO_4F \cdot 2H_2O$ like its sulfate homologue appear inactive toward the removal of Na as verified by the assembly of $NaCoSeO_4F \cdot 2H_2O$/Na cells using a 1 M $NaClO_4$ solution in Propylene Carbonate and tested by means of a Mac Pile system. It also displays poor ionic conductivity on the order of $\sigma = 10^{-12}$ S cm^{-1}.

dx.doi.org/10.1021/ic200700r |*Inorg. Chem.* 2011, 50, 7662–7668

Table 4. Selected Interatomic Angles and Distances Relevant to the Magnetic Properties[a]

	$NaCoSO_4F \cdot 2D_2O$	$NaCoSeO_4F \cdot 2H_2O$
NN M—M distance (Å)	3.66125(7)	3.7050(3)
interchain distance (Å)	5.73991(6)	5.8235(3)
interchain distance (Å)	7.19288(8)	7.3973(4)
M—F—M (deg)	131.5(1)	133.7(2)
M—F (Å)	2.007(1)	2.015(4)

[a] NN refers to the nearest-neighbour distance which occurs down the length of the chain. Note that there are two interchain distances, one along the *a*-axis and one along the *c*-axis. The values for the sulfate compounds were taken from the results of the refinement against the neutron diffraction data of the deuterated sample.

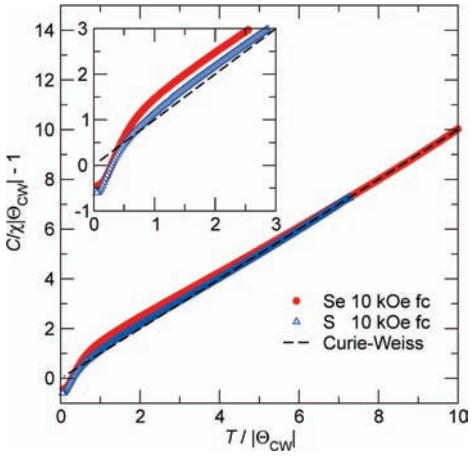

Figure 5. Inverse magnetic susceptibility normalized as described in the text. The filled red circles show the behavior of the selenate phase while the unfilled blue triangles show the sulfate phase. The dashed line illustrates the expected behavior for a system which follows ideal Curie—Weiss behavior. Note that the deviations (blown up to emphasize in the inset) above the dashed line could be reflective of short-range antiferromagnetic correlations.

RESULTS AND DISCUSSION

The temperature dependence of the magnetic susceptibility for the sulfate phase is shown in Figure 3 while the susceptibility of the selenate is shown in Figure 4. Both compounds show a peak around 4 K, which is indicative of the onset of antiferromagnetic ordering when cooled in a field of 100 Oe. There is a significant difference in the sharpness of this peak between the selenium- and sulfur-based phases. Interestingly, the cusp in both phases begins to be suppressed when the field is increased to 10 kOe.

The high temperature region (200 to 300 K) of the magnetic susceptibility collected in the 10 kOe field was fit to the Curie—Weiss equation, $C/(T - \Theta_{CW})$ to obtain the effective moment (μ_{eff}) from the Curie constant and the Curie—Weiss temperature, Θ_{CW}. An effective moment of 5.16 μ_B per Co is found for the sulfate whereas the effective moment of the selenate is closer to 4.70 μ_B per Co. These values can be compared with the 5.20 μ_B expected for a single Co^{2+} in an octahedral coordination environment (d^7, $t_{2g}^5e_g^2$, $S = 3/2$, $L = 3$) where an unquenched orbital moment which is fully decoupled from the spin contribution is present and can be calculated using the equation, $\mu_{L+S} = (4S(S + 1) + L(L + 1))^{1/2}$. In contrast, systems which have a completely quenched orbital contribution are expected to have a spin-only effective moment of 3.87 μ_B, which is obtained using the equation $\mu_s = 2(S(S + 1))^{1/2}$. Typical values for the effective moment of octahedral Co^{2+} sit anywhere in the range of 4.7—5.2 μ_B[12—14] depending on the degree of hybridization with the surrounding anions as determined by the degree of distortion to the octahedral environment.[15]

A Curie—Weiss temperature of −29 K is obtained for the selenate while the sulfate-based phase gives a value of −41 K. Given that the Curie—Weiss Θ reflects the relative strength of the dominant magnetic interactions, this difference is consistent with the idea that the shorter length of the M-F-M superexchange pathway in the sulfate phase, see Table 4, results in a larger degree of orbital overlap and hence a stronger interaction. Also considering that the magnetic interactions can be expected to be one-dimensional as a consequence of the crystal structure, this indicates that neighboring cobalt ions along the length of each chain most likely order antiferromagnetically with respect to each other and is supported by the neutron diffraction data which will be presented later.

The field cooled (FC) susceptibility collected in a field of 10 kOe, scaled using the values of C and Θ_{CW} obtained from the fit to the inverse susceptibility, is shown in Figure 5. The scaling is performed by plotting $C/(\chi|\Theta_{CW}|) - 1$ as a function of $T/|\Theta_{CW}|$, for which the Curie—Weiss behavior should yield a straight line through the origin (indicated by the dashed line) for a negative value of Θ_{CW}. Plotting in this manner emphasizes deviations from purely Curie—Weiss behavior. The usefulness of this type of scaling has been discussed in detail elsewhere.[16] It can be seen that in large fields the susceptibility begins to deviate from Curie—Weiss behavior well above the ordering temperature of 4 K. The positive sign of the deviations can be attributed to short-range antiferromagnetic correlations running along the length of the chain which develop above the ordering temperature. It should also be noted that the data collected in a field of 100 Oe gives qualitatively the same temperature dependence as the data collected in a field of 10 kOe.

The ratio of the Curie—Weiss Θ to the ordering temperature (Θ_{CW}/T_N) is greater than 7 for both compounds, suggesting a moderately suppressed ordering temperature which may be a reflection of multiple magnetic interactions competing to determine the ground state. In addition to the dominant superexchange through the *M*-F-*M* bonds, one must also consider the through-space dipolar interaction which will determine how chains align with each other. Additionally, the XO_4 units bridge the nearest-neighbor octahedra along the length of the chain. Such an arrangement gives rise to supersuperexchange (*M*-O-O-*M*) pathways which have been demonstrated to play an important role in determining the magnetic properties of other polyanionic compounds.[17—20]

Upon ordering, it can be seen that the curves in both compounds deviate strongly downward and eventually below the line marking ideal Curie—Weiss behavior. This behavior is indicative of some residual magnetic moment that is not fully compensated within the magnetic ground state. Such an uncompensated moment could be the result of a canted antiferromagnetic arrangement of the spins which is very common in Co-based magnetic systems because of the large degree of magnetocrystalline anisotropy associated with octahedral cations with a d^7 spin configuration.

dx.doi.org/10.1021/ic200700r |*Inorg. Chem.* 2011, 50, 7662–7668

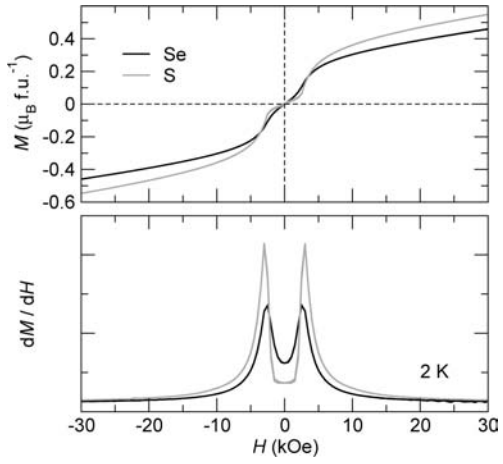

Figure 6. Top panel: isothermal magnetization curves for the sulfate and selenate phases obtained at 2 K. Bottom panel: derivative of the magnetization as a function of field. Note that the field-induced transition is significantly sharper for the sulfate than for the selenate.

To further probe the field dependence of the magnetic order, isothermal magnetization curves were collected at 2 K and are illustrated in the top panel of Figure 6. Starting around 3 kOe a sharp field-induced magnetic transition is observed in the sulfate phase, the details of which can be seen more clearly by examining the derivative of the magnetization which is illustrated in the bottom panel of Figure 6. Much like in the temperature dependence of the susceptibility, the sharpness of the field-induced transition is much less sharp in the selenate phase than in the sulfate. This seems to be consistent with the notion that the selenate has a weaker dominant exchange interaction since the transition in the selenate phase starts to develop even at very small fields.

To better understand the magnetic ground state, powder neutron diffraction patterns of deuterated $NaCoSO_4F \cdot 2D_2O$ were collected above (10 K) and below (1.6 K) the magnetic ordering temperature. Sufficient quantities of $NaCoSeO_4F \cdot 2D_2O$ to yield good quality diffraction patterns could not be produced, so all of the discussion on the neutron diffraction results pertain strictly to the sulfate analogue. Because of the close structural similarities and magnetic properties, it is reasonable to expect that the magnetic structure of the selenate will be very similar to that of the sulfate.

Upon passing through the Néel temperature of 4 K, several tiny additional peaks are found in the diffraction patterns recorded at 1.6 K. These peaks are difficult to see, in part because of the large incoherent neutron-scattering cross-section of cobalt (4.8 barns) in addition to the very close proximity to the Néel temperature. To be sure that these peaks were truly associated with long-range magnetic order and were not simple experimental artifacts, two separate wavelengths were used. A wavelength of 1.594 Å was chosen to solve the nuclear structure (including deuterium positions) whereas a wavelength of 2.398 Å was used to more clearly distinguish magnetic reflections at large *d*-spacing. Long acquisitions were collected on both a deuterated and nondeuterated sample at 10 K as well as 1.6 K which was the lowest accessible temperature the cryostat could reach. The nondeuterated sample was used as a reference to ensure that the Néel temperature had not shifted with the exchange of deuterium for hydrogen.

By plotting the difference between the patterns recorded above (10 K) and below (1.6 K) the ordering temperature for both hydrated and deuterated samples, it becomes apparent that there are three new and distinct Bragg peaks which occur at *d*-spacings of 5.98 Å, 5.03 Å, and 4.00 Å. It is worth noting that aside from the Co−F−Co superexchange pathway each chain is relatively isolated from the others, but despite this fact the clear presence of magnetic reflections confirms the long-range character of the overall ground state.

These three magnetic peaks could not be indexed within the unit cell which describes the nuclear structure. Attempts were therefore made to determine if simple propagation vectors within the first Brillouin zone could account for the reflections. It was immediately clear that only two special **k**-vectors could accurately index these peaks: $\mathbf{k} = (^1/_2\ 0\ 0)$ or $\mathbf{k} = (^1/_2\ 0\ ^1/_2)$. These two propagation vectors generate peaks at identical positions with two other possible reflections at high *d*-spacings of 6.94 Å and 10.48 Å, but no change in intensity was found at these latter two positions below T_N.

In the title compounds, the two cobalt atoms are distributed on the 2*d* Wyckoff site of the $P2_1/m$ space group at positions $(^1/_2\ 0\ ^1/_2)$ and $(^1/_2\ ^1/_2\ ^1/_2)$, that is, two adjacent cobalt ions in the chain. The different possibilities of magnetic configurations were investigated using Bertaut's method as implemented in Basireps[21,22] which reduces the number of allowable orientations of the moments to obey the symmetry of the space group. The total magnetic representation for each of the two possible propagation vectors can be decomposed into two irreducible representations, each consisting of three basis vectors. For $\mathbf{k} = (^1/_2\ 0\ 0)$ $\Gamma = 3\Gamma_2 + 3\Gamma_4$, leading to two possible spin configurations:

$$\Gamma_2:\ F^X = {S_1}^X + {S_2}^X;\ A^Y = {S_1}^Y - {S_2}^Y;\ F^Z = {S_1}^Z + {S_2}^Z$$

$$\Gamma_4:\ A^X = {S_1}^X - {S_2}^X;\ F^Y = {S_1}^Y + {S_2}^Y;\ A^Z = {S_1}^Z - {S_2}^Z$$

Whereas for $\mathbf{k} = (^1/_2\ 0\ ^1/_2)$, $\Gamma = 3\Gamma_1 + 3\Gamma_3$, leading to two possible spin configurations:

$$\Gamma_1:\ A^X = {S_1}^X - {S_2}^X;\ F^Y = {S_1}^Y + {S_2}^Y;\ A^Z = {S_1}^Z - {S_2}^Z$$

$$\Gamma_3:\ F^X = {S_1}^X + {S_2}^X;\ A^Y = {S_1}^Y - {S_2}^Y;\ F^Z = {S_1}^Z + {S_2}^Z$$

where S_i^X is the component along *x* of the magnetic moment of atom (*i*). For example, the representation Γ_1 corresponds to a ferromagnetic coupling of the two moments in the *y* direction (F^Y), while in the *x* and *z* directions (A^X and A^Z), the moments are coupled antiferromagnetically.

The small intensity of the magnetic reflections do not give enough information to accurately refine the magnetic structure using least-squares methods. However, simulations of neutron diffraction patterns for various simple model magnetic structures were computed and proved informative in determining which configurations could generate peaks at the correct positions while excluding intensity at higher *d*-spacings (6.94 Å and 10.48 Å) where no reflections were observed. Simulations where the moments aligned along the direction of the chains (i.e., moments along **b** only), or moments perpendicular to the chains [moments in the (**a**,**c**) plane] were also computed.

Such an approach yields four possible ground states:

- $\mathbf{k} = (^1/_2\ 0\ 0)$ and Γ_4, moments perpendicular to the chains (in the **a**,**c** plane)
- $\mathbf{k} = (^1/_2\ 0\ 0)$ and Γ_2, moments parallel to the chains (along **b**)

dx.doi.org/10.1021/ic200700r |*Inorg. Chem.* 2011, 50, 7662–7668

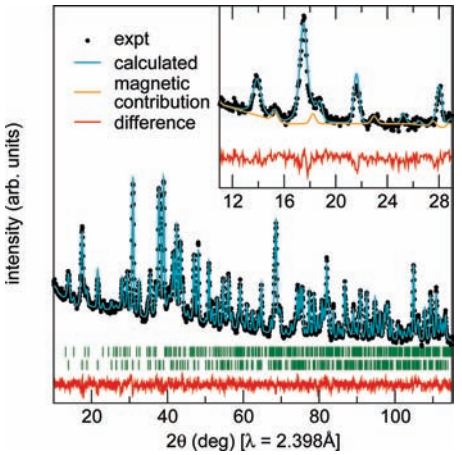

Figure 7. Rietveld refinement with the magnetic model presented in Figure 8, of the powder neutron diffraction pattern of the deuterated $NaCoSO_4F \cdot 2D_2O$ sample collected at 1.6 K. The black dots are experimental points while the blue and red lines are the calculated fit and the difference curve, respectively. The top set of green vertical marks show the location of nuclear reflections whereas the bottom row shows the expected position of magnetic reflections. Note that the magnetic contribution (orange line) to the pattern is very small as a result of the close proximity to the Néel temperature of 4 K, which makes precise determination of the orientation of the magnetic moment difficult.

- $\mathbf{k} = (^1/_2\ 0\ ^1/_2)$ and Γ_1, moments perpendicular to the chains (in the **a**,**c** plane)
- $\mathbf{k} = (^1/_2\ 0\ ^1/_2)$ and Γ_3, moments parallel to the chains (along **b**)

Examination of these four possible magnetic structures showed that the common feature for all cases is that the moments along the length of the chains always align antiparallel with the absolute orientation of the moment in space pointing either parallel or perpendicular to the length of the chain. Since the nuclear unit cell contains only a single chain, the propagation vector, $\mathbf{k} = (^1/_2\ 0\ 0)$, necessarily dictates that the antiferromagnetic chains are coupled ferromagnetically along the **c** direction. In contrast, $\mathbf{k} = (^1/_2\ 0\ ^1/_2)$ implies that all the chains are antiferromagnetically coupled. Since there is no structural difference in the **a** or **c** direction there is no reason, a priori, to believe that the magnetic coupling will be different between those unit cell edges. Therefore, the propagation vector $\mathbf{k} = (^1/_2\ 0\ ^1/_2)$ is more reasonable. Co^{2+} has a strong magnetocrystalline anisotropy where the angular momentum is not quenched as evidenced in the addition to the magnetic moment found on each Co atom. This is a common feature in Co^{2+} compounds, as discussed earlier, and is also found in Fe^{2+} compounds.[23,24] As a consequence, it is most likely that the moments on the Co^{2+} will align along the local pseudosymmetry axes of the octahedron rather than along the cell axis. It is therefore believed that the most probable ground state magnetic structure would be that which results from Γ_1 with $\mathbf{k} = (^1/_2\ 0\ ^1/_2)$, which predicts that the moments lay perpendicular to the chains in the **a**,**c** plane. A refinement of the 1.6 K pattern using this magnetic model is presented Figure 7, and the magnetic structure is illustrated in Figure 8. The magnetic moment to account for the intensity of the observed magnetic peaks is estimated to 1.9(2) μ_B which can be contrasted against the 3−4 μ_B usually observed for Co^{2+} in an octahedral environment. This underestimate is most likely because the moment has not yet fully saturated 2−3 K below

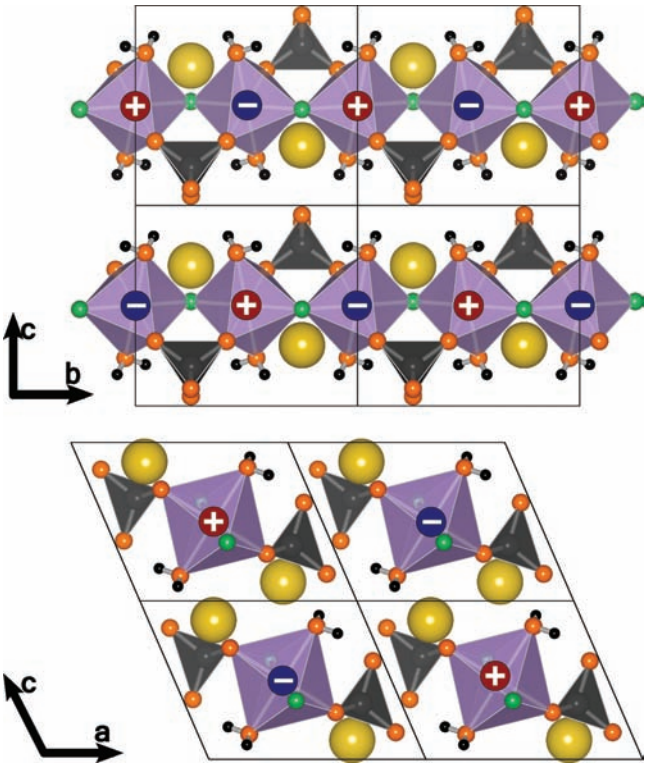

Figure 8. Illustration of the proposed magnetic structure of $NaCoSO_4F \cdot 2D_2O$. Co atoms in purple, O in orange, F in green, Na in yellow, H in black, and Se in dark gray. The crystal structure is identical to that of $NaCoSeO_4F \cdot 2H_2O$. Note that since the precise orientation of the magnetic moment could not be determined, we denote the up and down spins simply as a + or − on each atom. The ground state magnetic structure corresponds to a G-type antiferromagnet where all of the spins are oriented antiparallel to each other.

T_N. If one considers this compound in a perovskite-like topology the magnetic structure we propose corresponds to a G-type ground state where all the spins in all directions are coupled antiferromagnetically.

Considering that the ground state magnetic structure is G-type in character allows one to speculate on the nature of the field-induced magnetic transition. Given that there are no ferromagnetic interactions involved in establishing a G-type antiferromagnet, it is unlikely that the field-induced transition corresponds to a change from an antiferromagnetic to ferromagnetic state. This is further supported by the fact that the saturation magnetization appears to only approach a value on the order of 0.5 μ_B f.u.$^{-1}$ at 50 kOe in both compounds. Together these two observations appear to support the possibility that the presence of large magnetic fields results in a disruption of the long-range magnetic order which results in a paramagnetic state. Such an antiferromagnetic to paramagnetic transition in strong fields has been previously reported in similar highly anisotropic single molecule magnetic systems.[25]

We also remark that the selenate can be dehydrated at temperatures greater than 200 °C to give the first ever reported $NaCoSeO_4F$, which crystallizes in a monoclinic unit cell, with lattice parameters a = 6.8402(3) Å, b = 8.8918(3) Å, c = 7.2513(3) Å, β = 114.448(2)°, V = 401.50(3) Å^3. This new phase is currently under investigation as a potential positive electrode.

dx.doi.org/10.1021/ic200700r |*Inorg. Chem.* 2011, 50, 7662–7668

CONCLUSIONS

Here we have presented the synthesis and structural characterization of two previously uncharacterized compounds: $NaCoXO_4F \cdot 2H_2O$ (where X = S or Se). We have shown that in the absence of external magnetic fields both compounds undergo transitions to antiferromagnetic structures around 4 K. Using low temperature powder neutron diffraction we determined that the magnetic structure of $NaCoSO_4F \cdot 2H_2O$ corresponds to a G-type antiferromagnet in which all of the spins are antiferromagnetically coupled. The presence of large magnetic fields is found to result in a field-induced magnetic transition which is believed to result in a paramagnetic state.

ASSOCIATED CONTENT

Supporting Information. Crystallographic data in CIF format. This material is available free of charge via the Internet at http://pubs.acs.org.

AUTHOR INFORMATION

Corresponding Author
*E-mail: jean-marie.tarascon@sc.u-picardie.fr.

ACKNOWLEDGMENT

The authors thank Juan Rodríguez-Carvajal for fruitful discussions and Michela Brunelli for help with data collection at ILL. The authors also gratefully acknowledge the Seshadri group at UCSB for assistance with magnetic measurements which were supported by funding from the National Science Foundation through a MRSEC award (DMR 0520415).

REFERENCES

(1) Loiseau, Th.; Calage, Y.; Lacorre, P.; Ferey, G. *J. Solid State Chem.* **1993**, *111*, 390–396.
(2) Beitone, L.; Guillou, N.; Millange, F.; Loiseau, Th.; Ferey, G. *Solid State Sci.* **2002**, *4*, 1061–1065.
(3) Pereira, N.; Badway, F.; Wartelsky, M.; Gunn, S.; Amatucci, G. G. *J. Electrochem. Soc.* **2009**, *156*, A407–A416.
(4) Bervas, M.; Klein, L. C.; Amatucci, G. G. *J. Electrochem. Soc.* **2006**, *153*, A159–A170.
(5) Recham, N.; Chotard, J.-N.; Dupont, L.; Delacourt, C.; Walker, W.; Armand, M.; Tarascon, J. M. *Nat. Mater.* **2010**, *9*, 68–74.
(6) Sabelli, C. *B. Mineral.* **1985**, *108*, 133–138.
(7) Ati, M.; Dupont, L.; Recham, N.; Chotard, J.-N.; Walker, W. T.; Davoisne, C.; Barpanda, P.; Sarou-Kanian, V.; Armand, M.; Tarascon, J. M. *Chem. Mater.* **2010**, *22*, 4062–4068.
(8) Melot, B. C.; Goldman, A.; Darago, L. E.; Furman, J. D.; Rodriguez, E. E.; Seshadri, R. *J. Phys.: Condens. Mater.* **2010**, *22*, 506003.
(9) Uzunova, E.; Klissurski, D.; Mitov, I.; Stefanov, P. *Chem. Mater.* **1993**, *5*, 576–582.
(10) Rodríguez-Carvajal, J. *Phys. B* **1993**, *192*, 55, see http://www.ill.eu/sites/fullprof/.
(11) Rietveld, H. M. *J. Appl. Crystallogr.* **1969**, *2*, 65.
(12) Hulvey, Z.; Melot, B. C.; Cheetham, A. K. *Inorg. Chem.* **2010**, *49*, 4594–4598.
(13) Feller, R. K.; Melot, B. C.; Forster, P. M.; Cheetham, A. K. *J. Mater. Chem.* **2009**, *19*, 2604–2609.
(14) Melot, B. C.; Paden, B.; Seshadri, R.; Suard, E.; Nénert, G.; Dixit, A.; Lawes, G. *Phys. Rev. B* **2010**, *82*, 014411.
(15) Smura, C. F.; Parker, D. R.; Zbiri, M.; Johnson, M. R.; Gál, Z. A.; Clarke, S. J. *J. Am. Chem. Soc.* **2011**, *133*, 2691–2705.
(16) Melot, B. C.; Drewes, J. E.; Seshadri, R.; Stoudenmire, E. M.; Ramirez, A. P. *J. Phys.: Condens. Matter* **2009**, *21*, 216007.
(17) Melot, B. C.; Rousse, G.; Chotard, J.-N.; Ati, M.; Rodrguez-Carvajal, J.; Kemei, M. C.; Tarascon, J.-M. *Chem. Mater.* **2011**, *23* (11), 2922–2930.
(18) Rousse, G.; Rodríguez-Carvajal, J.; Wurm, C.; Masquelier, C. *Chem. Mater.* **2001**, *13*, 4527–4536.
(19) Rousse, G.; Rodríguez-Carvajal, J.; Wurm, C.; Masquelier, C. *Solid State Sci.* **2002**, *4*, 973–978.
(20) Rousse, G.; Rodríguez-Carvajal, J.; Patoux, S.; Masquelier, C. *Chem. Mater.* **2003**, *15*, 4082–4090.
(21) Bertaut, E. F. *Acta Cryst.* **1968**, *A24*, 217–231.
(22) Rodríguez-Carvajal, J. *BASIREPS-A Program for Calculating Non-Normalized Basis Functions of the Irreductible Representations of the Little Group Gk for Atom Properties in a Crystal*; Laboratoire Leon Brillouin, CEA Saclay: Gif sur Yvette, France, 2004.
(23) Rousse, G.; Rodríguez-Carvajal, J.; Patoux, S.; Masquelier, C. *Chem. Mater.* **2003**, *15*, 4082–4090.
(24) Melot, B. C.; Rousse, G.; Chotard, J.-N.; Ati, M.; Rodríguez-Carvajal, J.; Kemei, M. C.; Tarascon, J.-M. *Chem. Mater.* **2011**, *23*, 2922−2930.
(25) Harris, T. D.; Coulon, C.; Clérac, R.; Long, J. R. *J. Am. Chem. Soc.* **2011**, *133*, 123–130.
(26) Brown, I. D.; Altermatt, D. *Acta Cryst.* **1985**, *B41*, 244–247.

NOTE ADDED AFTER ASAP PUBLICATION

This paper was published on the Web on July 12, 2011, with an error in Figure 1. The corrected version was reposted on July 15, 2011.